

ERS: a novel comprehensive endoscopy image dataset for machine learning, compliant with the MST 3.0 specification

Jan Cychnerski  Tomasz Dziubich  Adam Brzeski 

Department of Computer Architecture
Gdańsk University of Technology
Narutowicza 11/12, Gdańsk, Poland

September 1, 2021

Abstract

The article presents a new multi-label comprehensive image dataset from flexible endoscopy, colonoscopy and capsule endoscopy, named ERS. The collection has been labeled according to the full medical specification of 'Minimum Standard Terminology 3.0' (MST 3.0), describing all possible findings in the gastrointestinal tract (104 possible labels), extended with an additional 19 labels useful in common machine learning applications.

The dataset contains around 6000 precisely and 115,000 approximately labeled frames from endoscopy videos, 3600 precise and 22,600 approximate segmentation masks, and 1.23 million unlabeled frames from flexible and capsule endoscopy videos. The labeled data cover almost entirely the MST 3.0 standard. The data came from 1520 videos of 1135 patients.

Additionally, this paper proposes and describes four exemplary experiments in gastrointestinal image classification task performed using the created dataset. The obtained results indicate the high usefulness and flexibility of the dataset in training and testing machine learning algorithms in the field of endoscopic data analysis.

Keywords: *medical dataset, image recognition, digestive tract endoscopy, machine learning, minimal standard terminology*

1 Introduction

The importance and extent of potential benefits from the use of sophisticated information systems in medicine give strong motivation for research on new possibilities of supporting medical examinations. One of the significant directions of research is the development of automatic analysis tools, not only for image, but also offline and on-the-fly analyzing video streams. One of the examples

of such fields is an endoscopic examinations of a human gastrointestinal (GI) tract, which is a very important medical procedure in the diagnosis of GI diseases. Diseases of the digestive system comprised of 4% of the total number of causes of death in 2016 in the EU [1]. Only colorectal cancer patients comprise of 10.2% of the total number of new cases in 2018 in the world. In Europe, there were near 500 000 new cases of cancer incidence and mortality exceeded over 250 000 [2]

By enabling the examination of the interior of the digestive tract, cancer can be detected at an early stage, which in turn gives a good chance of an effective treatment.

The modern field of endoscopy, which has been developing rapidly in the last two decades, is the Wireless Capsule Endoscopy (WCE). This examination involves the patient swallowing capsule measuring ca. 9x26mm, equipped with a camera and a light source. The recorded images are transmitted wirelessly to a receiver located on the waist around the patient's hips. The result of the examination is a video that is then analyzed by an expert. Unfortunately, the specifics of such films make the analysis very time-consuming - for typical, eight-hour recording it usually takes about 1-2 hours. This is the most difficult task that requires the physician to work in continuous concentration and continuous focus on the image [3]. The only indications for the doctor are the information provided by the patient during the medical history. Moreover, during a video colonoscopy, up to 26% of polyps can be overlooked, depending on: the endoscopist skills, the time of the exam (part of a day), the quality of colon preparation, visibility (some polyps are behind folds and difficult to detect), the size of the polyps (at early stage, some polyps could be flat and difficult to identify from normal intestinal mucosa) [4].

There is, therefore, a need for a decision support system in the analysis process, which would also allow us to shorten the process and save time for the specialist. The system should conduct a preliminary analysis of the film material examined to indicate fragments of the film depicting medical suspicion of lesions.

One of the common problems in GI endoscopy field is the detection of the occurrence of bleeding and polyps. Commercial solutions offered by the producers are based on Suspected Blood Indicator determination (SBI) that is related in straightway to a level of red color into image. Several robust techniques have been described in the literature to support these processes. The comprehensive review can be found in [5], but in spite of passing of time none of the mentioned techniques have been widely commercialized. In this paper, none of deep learning techniques were presented, which nowadays are a growing trend in general data analysis. Classification accuracy of the developed deep learning approaches is quantitatively compared (or even better) with traditional digital image analysis methods requiring prior computation of handcrafted features, such as statistical measures using gray level co-occurrence matrix, Gabor filter-bank responses, LBP histograms, gray histograms, HSV histograms and RGB histograms, followed by traditional machine learning methods [6]. Currently, most solutions utilize other ML techniques (so-called conventional ML) among

which the leading ones are SVM, Logit-regression. They are able to solve the task with relatively small training data set. However, the modern trend is deep learning (DL) methods and especially Convolutional Neural Networks (CNN). The achieved accuracy is at the level of ca.92% and sensitivity - ca.85%. It shows that DL methods can compete with classical methods [7, 8]. The most relevant studies in deep learning for polyp detection and classification in colonoscopy could be found at [9].

A large data training set of valuable data plays a crucial role in DL approach but it is frequently hard to access and most researchers in the medical field are tentative to practice open data science for reasons such as the risk of data misuse by other parties and lack of data-sharing incentives. On the other hand, there is no universal protocol to model, compare, or benchmark the performance of various data analysis strategies [10]. Data sets containing medical images are hardly available, making reproducibility and comparison of approaches almost impossible.

In this paper we present a large data set for creating and benchmarking machine learning algorithms that support medical diagnostics. Our goal was to create the data set in the field of GI endoscopy (colono- as well as gastroscopy), both traditional and WCE. We tried to get all classes encountered in Minimal Standard Terminology 3.0 [11], a gold standard platform for the multitude of endoscopic report generators for many years. To our knowledge it is the first such public set in the world. It consists of over 115 000 images divided into 99 classes with accordance to MST terminology. The remainder of this paper is structured as follows: a review of existing atlases and data sets of images and videos in endoscopy is given in section II. Next, our data set is described in details. In section IV we provide a quantitative assessment of deep learning algorithms for a wide range of diseases and artifacts classification. Finally, section V contains a summary and a conclusion.

2 Related works

One of the problems occurring in the process of creating automated classifiers based on deep convolutional neural networks (DCNN) is the acquisition of a training data set that has appropriate size [12]. In our paper we propose to come to grips with the problem of automated multi-class classification of GI tract diseases through the application of a DCNN architecture. Hence we need a set of at least thousands of images for a given class/disease. Some of them could be generated through augmentation techniques in a synthetic way. However, the quality of the data set is also essential, and it is crucial that all the images and videos are annotated correctly. Another potential issue in machine learning is over-fitting. A diverse data set is therefore recommended to better enable correct disease classification/detection in new data.

Existing web resources are relatively poor. Mostly, they contain dozen of images, usually with one pathology or photos of healthy organs and act as medical atlases. We can give as examples: El Salvador Gastroenterology Atlas with

5086 endoscopic videos [13] and Gastrolab - US National Endoscopic Database - 1498 images [14]. It is worth noting that many older atlases have disappeared (e.g. the Atlas of Gastrointestinal Endoscopy - Atlanta South Gastroenterology, US and the Atlas of Gastroenterological Endoscopy Departments of Internal Medicine of Finsterwalde Hospital and Aschersleben Hospital, Germany).

Specialized challenges are another more valuable source of endoscopic images and videos (i.e. MICCAI incl. Giana, Kaggle) which provide benchmark data sets that come with expert ground truth contours and standard evaluation measures to assess automated segmentation performance. In MICCAI 2015 challenge which covers a polyp segmentation in both colonoscopy images (SD and HD) and the tasks related to WCE image classification, ASU-Mayo data set was used. It is the first, largest, and a constantly growing set of short and long colonoscopy videos, collected and annotated at the Department of Gastroenterology at Mayo Clinic in Arizona. Currently this data set consists of 38 different, pixel-wise annotated videos (20 in training, 18 in testing set). Each image in this database comes with a ground truth image or a binary mask that indicates the polyp region. 20 short training colonoscopy videos of which 10 videos have a unique polyp inside and the other 10 videos have no polyps, HD (1920x1080) and SD (856x480, 712 x 480) resolutions. Data set consists of 18996 images and a total of 4278 polyp instances, testing set - 17575 in total and 4313 with polyps [15].

The ETIS-LARIB (ENSEA/CNRS/University of Cergy-Pontoise) data set contains 196 polyp images with a resolution of 1225x966 pixels in HD [16]. All images were extracted from 34 different colonoscopy videos which contain 44 unique polyps. The total number of polyps is 208. These data sets do not contain any “healthy” (normal) images and are usually used for testing.

The last data set used in the above-mentioned challenges was CVC-Clinic collections (subsets) shared by CVC-Clinic research group. It is being constantly developed; now it has reached the size of 11954 images. The first subset is CVC-ColonDB – a database of annotated image sequences of colonoscopy video with polyps. It contains 15 short colonoscopy videos, coming from 15 different examinations and provides annotations of the region of interest (ROI) for 300 images selected from all the videos (resolutions 500x574). These images were selected in order to maximise the visual difference between them. The ROIs define the whole area covering the polyp and they are implemented as binary images, with white masks over a black background. The database consists of 1706 different images, divided into four groups: original files (BMP format), polyp masks, non-informative region masks and contour of the polyp masks. The second one is CVC-ClinicDB2015 contains 612 images with associated polyp and background (here, mucosa and lumen) segmentation masks obtained from 31 polyp videos acquired from 23 patients (384x288) [17]. On the base of these two data sets, the new one CVC-EndoSceneStill was created, which extends the old annotations to account for lumen, specular highlights as well as a void class for black borders present in each image. In the new annotations, background only contains mucosa (intestinal wall) [18]. Additionally, it includes a test set with 44 videos from 36 patients and 912 images.

In [19] we could find a new data set, namely CVC–Clinic2017 (or CVC–12k), consists of 11954 images from 18 videos with one polyp (in total 10025 images) and test set - 18 videos with 18733 images. Each image that contains a polyp comes with pixel-wise annotations in the CVC–356 and CVC–612 data sets. It has to be noted that the ground truth in the CVC–VideoClinicDB data set represents an approximation of the polyp in the image using ellipses.

Kvasir is the largest data set in gastroscopy and consists of images, annotated and verified by medical doctors (experienced endoscopists), including several classes showing anatomical landmarks (Z-line, pylorus, cecum), pathological findings (esophagitis, ulcerative colitis, polyps) or endoscopic procedures in the GI tract; contains 8,000 images divided into 8 classes, 1,000 images for each class. In addition, authors provide several sets of images related to removal of lesions, e.g. ‘dyed and lifted polyp’, ‘dyed resection margins’, etc. The data set consist of the images with different resolution from 720x576 up to 1920x1072 pixels and organized in a way where they are sorted in separate folders named accordingly to the content. Some of the included classes of images have a green picture in picture illustrating the position and configuration of the endoscope inside the bowel, by use of an electromagnetic imaging system (ScopeGuide, Olympus Europe) that may support the interpretation of the image. This type of information may be important for further investigations (thus included), but must be handled with care for the detection of the endoscopic findings [20].

The next data set is called KiD and is divided into two sets: KiD1 and KiD2. It is an open academic access database of high quality annotated WCE video and images. (resolution of images 360x360 pixels). The first data set (KiD1) consists of a total of 77 images obtained using MiroCam® (IntroMedic Co, Seoul, Korea) capsule endoscopes. These images illustrate various types of abnormalities, including angioectasias, aphthae, chylous cysts, polypoid lesions, villous oedema, bleeding, lymphangiectasia, ulcers and stenoses. The second one (KiD2) comprise of 2371 WCE images. These images illustrate assorted small bowel findings including polypoid, vascular and, inflammatory lesions. This data set also includes normal images from the esophagus, stomach, small bowel and colon. Beside of this, there are three video data sets but they do not include annotations yet. Abnormalities depicted within this data set include 303 vascular (small bowel angiectasias and blood in the lumen), 44 polypoid (lymphoid nodular hyperplasia, lymphoma, Peutz–Jeghers polyps) and 227 inflammatory (ulcers, aphthae, mucosal breaks with surrounding erythema, cobblestone mucosa, luminal stenoses and/or fibrotic strictures, and mucosal/villous oedema) lesion images and 1778 normal images obtained from the esophagus, the stomach, the small bowel, and the colon [21].

All mentioned above data sets are available to the public either after registration or sending an inquiry.

An interesting data set was presented by [22]. They used huge data set consisting of 289 colonoscopy videos (156337 images, 60914 with polyps) from 151 patients with polyp history. Moreover the set contains a division into individual types and characteristics of polyps: carcinomatous, adenomatous, hyperplastic, inflammatory and small, isochromatic, flat. There is no information about type

of annotations. Unfortunately, this data set is not available in public.

A summary of mentioned data sets was presented in Tab. 1. As could be seen that vast majority of data sets are related to colonoscopy and we have deficiency of data in remaining categories of GI diseases and artifacts.

Table 1: Comparison of considered data sets.

Data set name	Modality	Videos / patients	Total number of images	Classes	Type of annotations	Number of normal images
CVC-ColonDB	colono-scopy	13/ 13	300 500×574	1 class (polyps) 300 images	corresponding ground-truth masks, non-informative region masks, contour of the polyp masks	0
CVC-Clinic2015 (CVC612)	colono-scopy	29/ 23	1962 384×288	1 class (polyps) 612 images	testing	1350 nonpolyp-image
CVC-EndoScene Still	colono-scopy	44/ 36	500×574 or 384×288	1 class 912	polyp, lumen, background, specularity, border (void)	combines ColonDB with Clinic2015 into a new data set with explicit divisions for train, test and validation set
CVC-Clinic2017	colono-scopy	18/ N/D	11954	1 class (polyps) 10025 polyp detection	graphical, imprecise oval shape covering whole polyp (approximated annotation)	1929 (second set - test 18 video with 18733 images)
KiD	WCE	47/ N/D	2500 360×360 + 47 video	Angiectasia, bleeding, inflammations, polyps		
Kvasir v2	gastro-scopy	N/A/ N/A	8000 from 720×576 up to 1920×1072	8 classes: Z-line, pylorus, cecum anatomical landmarks, pathological findings esophagitis, polyps, ulcerative colitis	image-wise annotations	N/A
ETIS-Larib Polyp DB	colono-scopy	34/ N/A	196 HD 1225×966	1 class (polyps) 44 different polyps with various sizes and appearances. At least one polyp existed in all 196 images, with the total number of polyps being 208	graphical pixel-wise annotations	0 polyp image
ASU-Mayo	colono-scopy	20 SD and HD (+18 test)/ N/A	18996 HD and SD	1 class (polyps) 4278	graphical pixel-wise annotations	14718
GIANA 2017	WCE	N/A/ N/A	1198 576×576	1 (angiodysplasia)	graphical, pixel-wise annotations	600
Nerthus	colono-scopy	21 /N/A	5525 720×576	4 (bowel)	classes showing four-score BBPS-defined bowel preparation quality the position and configuration of the endoscope inside the bowel.	1350

As it was shown in Tab. 1 most of data sets are addressed to one morbid entity or clinical findings, most often related to colonoscopy. The number of patients from whom the study comes is very low (up to several dozen). Images (and annotations) illustrate the same or very similar shoot of the disease, often from adjacent images. Most data sets do not provide pixel-wise annotations and the images are marked only with labels. This results in a rapid decrease in the suitability of them to semantic segmentation issues. Succeeding general problem is that several of the existing data sets are cumbersome to use in terms of permission are restricted.

The clean and complete data is one of the crucial parts of a good segmentation/object detection system. This means that spending the time to create a

high-quality data set is very important and is directly connected to the quality. These motivations drove us to creating a new large and complete data set called ERS (Endoscopy Recommendation System).

3 ERS dataset details

3.1 Dataset contents

In the MAYDAY 2012 project [23], carried out at the Gdansk University of Technology and the Medical University of Gdańsk (Clinic of Gastroenterology and Hepatology, GUMed), an attempt to create an ensemble of specialized classifiers of images from endoscopic videos was made. The aim of those classifiers, being a part of the MedEye application [24], was a multi-class classification and ROI detection to indicate places on the recording where the potential diseases occurred. This task is high-demand by clinicians during off-line WCE video analysis.

In order to accomplish this task we created a complex data set which consists of more than 6800 annotated images coming from retrospective endoscopic GI examinations. All cases were selected and annotated by physicians from the GUMed. We tried to span numerous set of endoscopic diagnosis, using terminology accordingly with Minimal Standard Terminology (MST 3.0) [11]. We collected and annotated images of 27 different types of colonoscopic findings (terms defined in MST chapter 5.2) and 54 of upper endoscopy findings (terms defined in MST chapter 5.1). The source videos originated from 1271 patient’s examinations (555 and 712 respectively).

In addition to MST-defined terms, in our data set we also included three other useful in (machine learning applications) categories of terms: healthy GI tract tissues, image quality attributes (such as sharp, blur, motion, stool etc.) and images containing blood. Description of all term categories in the data set is presented in Table 2.

Table 2: Categories of terms in our data set

Category	Category ID	Description	Number of terms
Gastro	g	All terms from MST 3.0 chapter 5.1 (upper endoscopy)	70
Colono	c	All terms from MST 3.0 chapter 5.2 (colonoscopy)	34
Healthy	h	Healthy tissues of upper endoscopy and colonoscopy	7
Blood	b	Information about blood presence in the endoscopic image	2
Quality	q	Information about quality and artifacts in the endoscopic image	10

Our data set is much more sophisticated than all other data sets presented in Table 1. It contains annotated data of 123 terms, divided into 5 categories. The overall number of images, annotations and patients is presented in Table 3. The detailed summary is presented in Table 4. In ‘Total’ column the number of images of specific term is given, whereas number of primary patient’s examinations is shown in ‘Number of patients’. Annotation masks were done by medical experts in a polygon-shaped forms (representing ROI for selected class; later converted to binary masks). For some annotations, mainly including healthy tissue or image quality, no such masks were used. Every annotation

was given a corresponding term. Number of such annotated images is shown in sub-column ‘Precise’ of Table 1. Note, that the table includes several rows with zeros, because our goal is to demonstrate the degree of compliance of our data set with the full MST specification.

Due to the fact that most of the images come from videos, which recording speed is about 30 frames per second, in the data set we also included images appearing up to few seconds before or after the annotated source video frame, if they are identical or very similar to the base image, and the annotation mask still fits visually the corresponding region of interest. However, it should be emphasized that this type of annotations/masks was not made by an expert, therefore we have placed them in a separate sub-column (‘Imprecise’). Although their lower accuracy, they can be useful in a deep neural network training due to their high abundance. Examples of ‘precise’ and ‘imprecise’ annotation masks are presented in fig. 1.

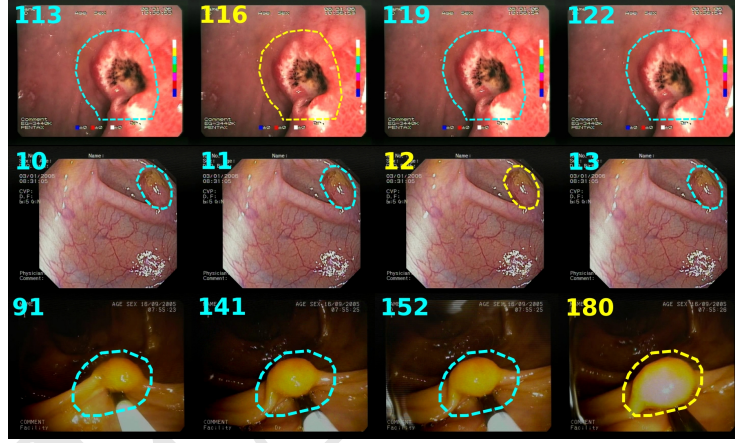


Figure 1: Precise (yellow) and imprecise (blue) annotation masks. In corners, frame ID in corresponding video sequence.

The total number of images in the category may differ from the sum of each term due to the possibility of multiple annotations for one image. Examples of collected images and annotations are presented in Appendixes.

The data set can be obtained at no charge for research purposes from:
<https://cvlab.eti.pg.gda.pl/publications/endoscopy-dataset>

Table 3: Data set summary: number of images, annotations and patients

Modality	Data summary	Images		Annotation masks		Number of patients	
		Precise	Imprecise	Precise	Imprecise	Precise	Imprecise
gastroscopy & colonoscopy	Total	5970	982041	3606	22671	1108	1119
	With at least one annotation	5970	115429	3606	22671	1098	918
	With no annotations	—	866612	—	—	10	201
WCE	Total	366656		—		7	

Table 4: Terms and number of annotations in our data set

Id	Category	Terms	Annotated images		Annotation masks		Number of patients	
			Precise	Imprecise	Precise	Imprecise	Precise	Imprecise
g	gastro	[total]	1779	21680	1790	8035	591	473
g02		achalasia	9	25	9	25	3	3
g03		barretts esophagus	20	119	20	119	8	7
g04		benign stricture	4	25	4	25	1	1
g05		bleeding of unknown origin	8	27	8	27	5	4
g06		coeliac disease	7	26	7	26	2	2
g07		crohns disease	6	37	6	37	1	1
g08		dieulafoy lesion	9	11	9	11	4	3
g10		duodenal bulb deformity	5	15	5	15	3	3
g11		duodenal cancer	19	37	19	37	5	3
g14		duodenal polyp	27	99	27	99	10	8
g15		duodenal postoperative appearance	1	—	1	—	1	—
g18		duodenal ulcer	106	436	106	436	44	34
g19		duodenal ulcer with bleeding	26	87	26	87	12	10
g20		duodenopathy:erosive	21	146	21	146	8	8
g22		duodenopathy:hyperemic	5	33	5	33	4	3
g25		esophageal caustic injury	5	12	5	12	2	2
g26		esophageal cancer	54	237	54	237	20	16
g27		esophageal candidiasis	12	144	12	144	3	3
g28		esophageal diverticulum	13	45	13	45	6	4
g29		esophageal fistula	17	76	17	76	8	8
g30		esophageal foreign body	5	1	5	1	2	1
g31		esophageal polyp	23	99	23	99	11	10
g32		esophageal postoperative appearance	1	—	1	—	1	—
g33		esophageal stricture	23	127	23	127	9	8
g35		esophageal submucosal tumor	3	6	3	6	1	1
g36		esophageal varices	170	466	170	466	66	55
g37		extrinsic compression	7	32	7	32	1	1
g39		gastric cancer	87	274	87	274	34	28
g40		gastric diverticulum	1	2	1	2	1	1
g41		gastric fistula	3	7	3	7	1	1
g42		gastric foreign body	19	65	19	65	10	8
g43		gastric caustic injury	2	1	2	1	2	1
g44		gastric lymphoma	20	31	20	31	7	5
g45		gastric polyp(s)	192	1210	192	1210	72	54
g46		gastric postoperative appearance	22	112	22	112	11	7
g47		gastric retention	18	27	18	27	7	2
g50		gastric ulcer	204	846	204	846	88	64
g51		gastric ulcer with bleeding	20	94	20	94	7	5
g52		gastric ulcer:anastomotic	17	24	17	24	10	7
g53		gastric varices	82	476	82	476	24	19
g54		gastropathy:erosive	83	446	83	446	31	23
g55		gastropathy:hemorrhagic	13	46	13	46	3	3
g56		gastropathy:hyperemic	33	510	33	510	17	12
g57		gastropathy:hypertrophic	2	12	2	12	1	1
g59		gastropathy:portal hypertensive	115	14385	115	631	46	47
g61		hiatus hernia	13	45	13	45	7	7
g62		mallory:weiss tear	16	43	16	43	8	6
g63		other esophagitis	95	335	95	335	37	31
g65		post sclerotherapy appearance	19	71	19	71	9	7
g66		pyloric stenosis	22	35	22	35	7	5
g67		reflux esophagitis	37	100	37	100	17	8
g68		schatzki ring	4	32	4	32	1	1
g69		scar	21	61	21	61	11	6
g70		submucosal tumor	24	131	24	131	6	4
c	colono	[total]	2199	37391	1635	14636	482	387
c01		angiodysplasia	61	597	61	597	14	13
c02		bleeding of unknown origin	5	5	5	5	3	2
c03		colitis:ischemic	20	54	20	54	5	4
c05		colorectal cancer	528	25345	270	2333	92	82
c08		crohns disease:active	127	1306	127	1306	19	16
c10		crohns disease:quiescent	18	151	18	151	11	9
c11		diverticulitis	1	6	1	6	1	1
c12		diverticulosis	83	325	83	325	29	16
c13		fistula	18	217	18	217	5	5
c14		foreign body	1	4	1	4	1	1
c15		hemorrhoids	11	65	11	65	5	4
c16		ileitis	3	13	3	13	1	1
c17		lipoma	12	113	12	113	3	3
c19		melanosis	19	75	19	75	6	6
c20		parasites	22	179	22	179	2	2
c22		polyp	950	5395	629	5395	247	185
c23		polyposis syndrome	16	220	16	220	7	4
c24		postoperative appearance	10	18	10	18	6	5
c25		proctitis	9	173	9	173	3	3
c26		rectal ulcer	22	510	22	510	8	7
c27		solitary ulcer	12	211	12	211	7	5
c28		stricture:inflammatory	1	6	1	6	1	1
c29		stricture:malignant	15	131	15	131	9	6
c30		stricture:postoperative	2	2	2	2	1	1
c31		submucosal tumor	2	8	2	8	1	1
c32		ulcerative colitis:active	162	1746	162	1746	33	28
c34		ulcerative colitis:quiescent	84	773	84	773	35	28
h	healthy	[total]	1019	19464	—	—	67	110
h01		esophagus	33	1006	—	—	6	13

h02		stomach	42	1214	–	–	6	29
h03		duodenum	29	1154	–	–	6	17
h05		small-bowel	4	65	–	–	1	1
h06		upper	9	8268	–	–	2	56
h07		colon	902	11129	–	–	49	53
b	blood	<i>[total]</i>	814	174	181	–	133	41
b01		blood	184	173	181	–	77	40
b02		no blood	630	1	–	–	56	1
q	quality	<i>[total]</i>	974	94470	–	–	97	224
q01		sharp	259	57530	–	–	3	172
q02		blur	428	36922	–	–	25	174
q03		bile	18	14	–	–	6	5
q04		food	1	–	–	–	1	–
q05		tooclose	82	50	–	–	23	15
q06		air	86	48	–	–	33	19
q07		defocus	51	25	–	–	27	18
q08		light	60	36	–	–	22	17
q09		motion	87	50	–	–	40	27
q10		stool	22	30	–	–	10	3

3.2 Dataset structure

The collection is stored in a form that makes it as easy and versatile as possible to use in a variety of machine learning problems. All visual data are stored as lossless compressed PNG files: endoscopic images as RGB images, annotation masks as monochrome PNG bitmaps. The labels (annotations) corresponding to the frames are included in the file names, and for convenience in the file `labels.csv`. Precise and imprecise masks and annotations are separated in distinct directories. Shortened IDs of all labels, along with descriptions are included in the file `names.json` and `names.csv`.

Patients. Due to the versatility of the dataset and the large number of unbalanced classes, a priori division of the data into training, validation and test sets is not possible. Such a division must be made by the researcher himself, taking into account the specifics of the problem he is investigating. In order to facilitate the construction of these sets, data are divided according to the patients they originate from. The data from each patient is stored in separate directories – to avoid bias, we recommend that data from a single patient never be simultaneously included in the training and test sets. The patients are numbered 0000 – 1135, and the directories containing the data are named as such.

Single frames and video sequences. The collection contains video sequences from endoscopic examinations and single frames cut from them. For each patient, there is one directory containing all *single* frames (`samples`) and several directories containing the video sequences (`seq_01`, `seq_02`, etc.). *Single* frames (`samples`) are mostly cut from video sequences – their annotations are *precise* (as defined in section 3.1). The frames in the movie sequences contain mostly *imprecise* annotations.

Endoscopic images. Each directory `samples` and `seq_N` contains a subdirectory `frames`, which includes the original endoscopic frames: color RGB images in PNG format. If present, personal information has been anonymized with black rectangles. The filename of each file corresponds to the frame number in the video sequence (e.g., `seq_01/frames/000215.png`) or the ordinal number of the cut *single* frame (e.g., `samples/frames/000001.png`).

Annotation files, labels, masks. If there are annotations for a given patient, the `samples` and `seq_N` directories contain the `labels` subdirectory.

This directory contains all annotations, labels, and masks for a given sequence or single images (samples). If any annotations exist for an image in the **frames** directory, they are located in the **labels** directory. Multiple annotation files may exist for each endoscopic image. Each annotation file is named according to convention: `[frame number]_[label 1]_[label 2]_[label...].png`. The frame number denotes the number of the corresponding annotated endoscopic image from the **frames** directory. An annotation file may contain multiple different label IDs in the name, separated by an underscore character – the label IDs are consistent with table 4 and the **names.csv** file. If the annotation is a mask, it is stored as a monochrome PNG file. If the annotation contains only labels (no mask) it is saved as an empty file (0 bytes in size). As mentioned earlier, the masks in the samples directories are *precise*, and in the **seq_N** directories they are *imprecise*.

An excerpt of the dataset directory tree is shown in fig. 2. Some exemplary files from the dataset along with an explanation are described below:

- `0025/samples/frames/000001.png` — cut single frame – endoscopic image of patient number 25
- `0025/samples/labels/000001_q05_q09.png` — annotation file for the above endoscopic image. It specifies two labels (q05 and q09). The file is empty (size of 0 bytes), so it does not contain an annotation mask.
- `0025/samples/labels/000003_g59.png` — annotation file for another endoscopic image `samples/000003.png`. It specifies the g59 label. The file is a monochrome PNG file, so it is an annotation mask of the g59 label. It is contained in the **samples** directory, so it is a *precise* mask.
- `0025/seq_01/frames/000185.png` — endoscopic frame 185 from video sequence 01 for patient 0025.
- `0025/seq_01/labels/000185_g59.png` — annotation for the above endoscopic frame – label g59. It is a monochrome PNG file, so it is an annotation mask. It is contained in the **seq_N** directory, so it is a *imprecise* mask.

4 Exemplary experiments using the dataset

In order to confirm the usefulness of the described data set, research on the efficiency of classifiers has been carried out. Our algorithms had been implemented in the form of single, universal models of a deep neural network (end-to-end approach). Three popular deep neural network architectures were used: Inception v3 [25], NASNet-Mobile [26] and MobileNet v1 [27]. The models were trained to recognize multiple classes at a time (multi-label classification, with threshold 0.5 on the output layer).

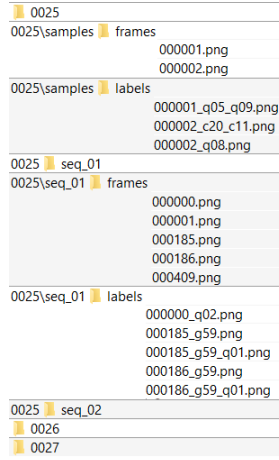


Figure 2: Fragment of the dataset directory tree

Four main problems were taken into account, as presented in Tab. 5. They reflect the different possible uses of target classifiers. The first of them (*10-CLASS*) can be used in screening, the next two in more accurate examination (*5-CLASS*, *2-CLASS*), directed at a specific group of diseases or a binary classification. The last (*BLUR*) one will allow us to discard blurry images from the recording, thus reducing the number of images to be viewed. Each class in the problems was built by combining several relevant terms from the data set (e.g. ‘normal tissue’ class was constructed using all ‘healthy’ terms). Exact recipes used to create the specific class, and resulting data set sizes were placed in Appendixes. On top of that, two variants of data were used to train the models: (1) only ‘precise’ images, and (2) both ‘precise’ and ‘imprecise’ images altogether. For testing, only ‘precise’ images were used.

Table 5: Description of four considered classification problems and data sets used during training process

Problem	Predicted classes	Variant	Training set		Testing set	
			Images	Patients	Images	Patients
10-CLASS	normal, blur, polyp, cancer, ulcer, blood, inflammation, crohn, diverticulum, varicose	Precise	4308	803	782	199
		Imprecise	88779	817	782	199
5-CLASS	normal, polyp, cancer, ulcer, blood	Precise	2954	586	559	133
		Imprecise	46835	610	559	133
2-CLASS	normal, disease	Precise	4098	874	901	216
		Imprecise	63102	885	901	216
BLUR	blur, sharp	Precise	4521	878	933	21
		Imprecise	90905	890	933	218

The data was split so as 80% of patients belong to ‘train’ subset, and 20% of patients to ‘test’ subset. In each data set, number of images for each class was balanced using repetition and augmentation (rotation, flip, color change, brightness change, blur). The number of patients and images per patient were not balanced, except for an additional ‘MobileNet-Balanced’ test in which the number of images per patient in each class was proportional to the square root of original number.

As a neural net efficiency metric, F-score based on sensitivity and specificity for each class was used. Final performances for whole network were calculated with macro-averaging (average over F-scores of individual classes). Results on test set for each neural network are presented in Fig. 3. For each problem, the best neural network found was used to calculate F-scores for individual classes in that problem, presented in Fig. 4.

The investigated problems, as predicted, showed different levels of difficulty. The most difficult problem was a 10-class problem, where the recognition of normal tissue, blurry image and varicose reached an F-score of 86–90%, and for diseases about 75–78% (except for Crohn’s disease and diverticulosis, probably due to a small number of training images). In the 5-class problem, F-score for diseases reaches 80–85%, and for healthy tissue 92%. A better result than in 10-class problem is due to fewer diseases analysed and no classes with a low number of training images. In 2-class problem 88% effectiveness was achieved in recognizing abnormal and healthy tissue. The lower effectiveness in recognizing healthy images than in 10-class and 5-class problems is due to the fact that in this problem, absolutely all diseases from the data set are analyzed, not just a subset of them. The simplest problem turned out to be the BLUR problem, where an F-score of 94% was obtained.

The conducted experiments do not indicate major differences in effectiveness between the tested neural networks. On average, MobileNet achieved slightly better results than other networks in most cases, and NASNet-Mobile was the worst. Noteworthy is a two-class problem, in which MobileNet achieved a significantly higher F-score than other networks (88%). At the same time, it was the only problem where the use of imprecise annotations resulted in significant improvement. The application of additional balancing of counts of images per patient also did not bring significant differences in network operation in any problem.

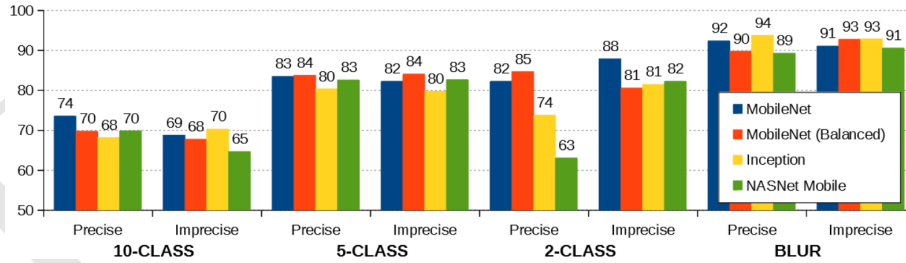


Figure 3: F-score (in %) for each neural network, for each problem and data set used.

In addition, we carried out the tests to estimate impact of using the MobileNet network (trained for 2-class problem described before) on video analysis time shortening by physicians. The classifier detects which video frames do not contain any anomalies and removes them, shortening the video length. The operation of the algorithm depends on the parameter of the desired sensitivity,

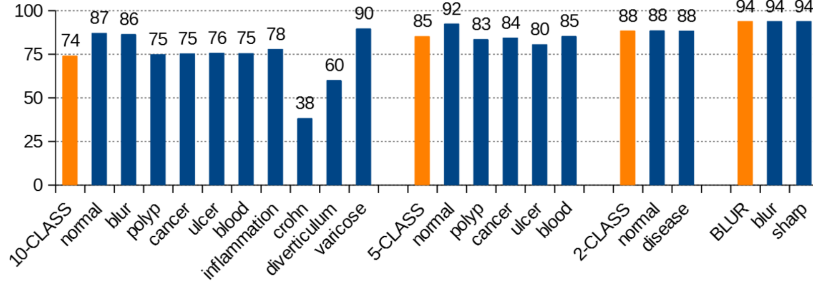


Figure 4: F-scores (in %) for each class in every problem considered, using best neural networks found (orange bar presents the average F-score over all classes).

which determines how many potential undetected anomalies the user is able to accept. For a parameter equal to 99% (which means the requirement to detect 99% anomalies), the video length has been reduced by 16%. With the reduction of this requirement, the film was additionally much shorter (by over 80%). It allows to shorten an examination time from about hours up to a few minutes (in case WCE examination). The relationship between the specified algorithm specificity and the obtained anomaly detection efficiency was also examined. The detailed results are presented in Fig. 5.

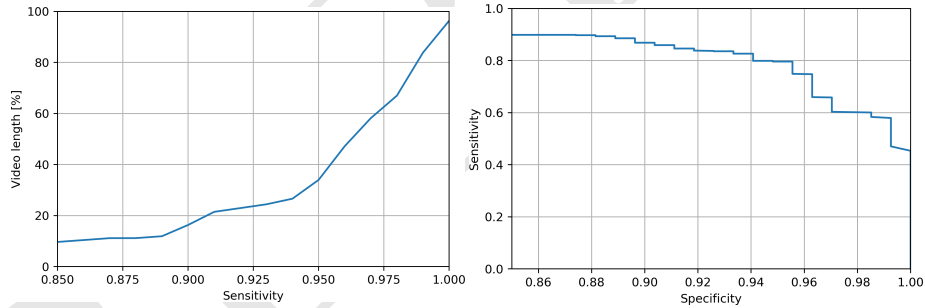


Figure 5: Video length after removing healthy images for specified anomaly detection sensitivity (left); sensitivity of anomaly detection for specified specificity (right).

5 Conclusions

In this paper we present a new large data set which could be useful in a training classifiers for computer-based diagnosis of GI tract. We also show a validation study comparing the performance of different CNN models for various class of problems. The review of the available data sets shows the need to create

a uniform, standardized research repository. The availability of large public collections, in particular in the field of gastroscopy, is very limited, and as important as colonoscopy. We believe that the presented ERS data set can be the foundation for such a benchmark platform. The study shows that access to large available annotated data is needed for a comprehensive validation of GI indications classification, detection and segmentation method and that this might lead to a boost in performance of end-to-end learning methods. The analysis of the results obtained for each class shows at a quite good performance in multi-class classification and superior at small number of classes, in both full-video sets and still images. For the multi-class classification, it shows how important the amount of collected data is (Crohn's disease has only 84 precise images whereas the set of diverticulum contains 135 and the set of polyps - 1192 images and their F-scores are 38, 60 and 86 respectively). The use of combination of different methods and algorithms shows that they are close to clinical use because it is able to select and order the most significant images in videos in a short time.

Acknowledgements

This research was partially funded by grants from National Centre for Research and Development (PBS2/A3/17/2013, Internet platform for data integration and collaboration of medical research teams for the stroke treatment centers).

References

- [1] Eurostat, Causes of death - deaths by country of residence and occurrence (2020).
URL https://appsso.eurostat.ec.europa.eu/nui/show.do?dataset=hlth_cd_aro&lang=en
- [2] Estimated cancer incidence, mortality and prevalence world-wide in 2018, http://gco.iarc.fr/today/data/factsheets/cancers/10_8_9-Colorectum-fact-sheet.pdf, WHO, World Health Organization – International Agency for Research on Cancer. (2018).
- [3] D. Hewett, C. Kahi, D. Rex, Efficacy and effectiveness of colonoscopy: how do we bridge the gap?, *Gastrointest Endosc Clin N Am.* 20 (2010) 673–684.
- [4] D. Ramsoekh, J. Haringsma, J. W. Poley, P. van Putten, H. van Dekken, E. W. Steyerberg, M. E. van Leerdam, E. J. Kuipers, A back-to-back comparison of white light video endoscopy with autofluorescence endoscopy for adenoma detection in high-risk subjects, *Gut* 59(3) (2010) 785–793.

- [5] A. Karargyris, N. Bourbakis, Wireless capsule endoscopy and endoscopic imaging: a survey on various methodologies presented., IEEE Engineering in Medicine and Biology Magazine 29(1) (2010) 72–83.
- [6] P. M. Szczypiński, A. Klepaczko, M. Kociolek, Qmazda—software tools for image analysis and pattern recognition, in: 2017 Signal Processing: Algorithms, Architectures, Arrangements, and Applications (SPA), IEEE, 2017, pp. 217–221.
- [7] H. Greenspan, B. van Ginneken, R. M. Summers, Guest editorial deep learning in medical imaging: Overview and future promise of an exciting new technique, IEEE Transactions on Medical Imaging 35 (5) (2016) 1153–1159. doi:10.1109/TMI.2016.2553401.
- [8] H. Shin, H. R. Roth, M. Gao, L. Lu, Z. Xu, I. Nogues, J. Yao, D. Mollura, R. M. Summers, Deep convolutional neural networks for computer-aided detection: Cnn architectures, dataset characteristics and transfer learning, IEEE Transactions on Medical Imaging 35 (5) (2016) 1285–1298. doi:10.1109/TMI.2016.2528162.
- [9] SING, Deep learning for polyp detection and classification in colonoscopy (2020).
URL <https://github.com/sing-group/deep-learning-colonoscopy>
- [10] I. D. Dinov, Methodological challenges and analytic opportunities for modeling and interpreting big healthcare data, Gigascience 5 (2016) 12. doi:10.1186/s13742-016-0117-6.
- [11] O. M. E. Digestive, Minimal standard terminology for gastrointestinal endoscopy, www.worldendo.org/assets/downloads/pdf/resources/mst/mst30.pdf.
- [12] G. Litjens, T. Kooi, B. E. Bejnordi, A. A. A. Setio, F. Ciompi, M. Ghafoorian, J. A. Van Der Laak, B. Van Ginneken, C. I. Sánchez, A survey on deep learning in medical image analysis, Medical image analysis 42 (2017) 60–88.
- [13] Julio Murra-Saca MD, El salvador atlas (2020).
URL gastrointestinalatlas.com
- [14] UNED, US National Endoscopic Database, Gastrolab - the gastrointestinal image site (2019).
URL gastrolab.net
- [15] N. Tajbakhsh, S. R. Gurudu, J. Liang, Automated polyp detection in colonoscopy videos using shape and context information, IEEE Transactions on Medical Imaging 35 (2) (2016) 630–644. doi:10.1109/TMI.2015.2487997.

- [16] J. Silva, A. Histace, O. Romain, X. Dray, B. Granado, Toward embedded detection of polyps in wce images for early diagnosis of colorectal cancer, *International journal of computer assisted radiology and surgery* 9 (2) (2014) 283–293. doi:10.1007/s11548-013-0926-3.
URL <https://doi.org/10.1007/s11548-013-0926-3>
- [17] J. Bernal, J. Sánchez, F. Vilarino, Towards automatic polyp detection with a polyp appearance model, *Pattern Recognition* 45 (9) (2012) 3166–3182.
- [18] D. Vázquez, J. Bernal, F. J. Sánchez, G. Fernández-Esparrach, A. M. López, A. Romero, M. Drozdal, A. Courville, A benchmark for endoluminal scene segmentation of colonoscopy images, in: *Journal of Healthcare Engineering*, 2017.
URL <https://arxiv.org/abs/1612.00799>
- [19] J. Bernal, H. Aymeric, Miccai endoscopic vision challenge polyp detection and segmentation (2017).
URL <https://endovissub2017-giana.grand-challenge.org/home/>
- [20] K. Pogorelov, K. R. Randel, C. Griwodz, S. L. Eskeland, T. de Lange, D. Johansen, C. Spampinato, D.-T. Dang-Nguyen, M. Lux, P. T. Schmidt, et al., Kvasir: A multi-class image dataset for computer aided gastrointestinal disease detection, in: *Proceedings of the 8th ACM on Multimedia Systems Conference*, 2017, pp. 164–169.
- [21] A. Koulaouzidis, D. K. Iakovidis, D. E. Yung, E. Rondonotti, U. Kopylov, J. N. Plevris, E. Toth, A. Eliakim, G. W. Johansson, W. Marlicz, et al., Kid project: an internet-based digital video atlas of capsule endoscopy for research purposes, *Endoscopy international open* 5 (06) (2017) E477–E483.
- [22] P. Wang, X. Xiao, J. Liu, L. Li, M. Tu, J. He, X. Hu, F. Xiong, Y. Xin, X. Liu, A prospective validation of deep learning for polyp auto-detection during colonoscopy: 2017 international award: 205, *American Journal of Gastroenterology* 112 (2017) S106–S110.
- [23] A. Blokus, A. Brzeski, J. Cychnerski, T. Dziubich, M. Jędrzejewski, Real-time gastrointestinal tract video analysis on a cluster supercomputer, in: *7th International Conference on Dependability and Complex Systems (DepCoS-RELCOMEX)*, 2012, pp. 55–68.
- [24] H. Krawczyk, P. Czarnul, T. Dziubich, Evaluation of multimedia applications in a cluster oriented environment, *Metrology and Measurement Systems* 2 (2012) 177–190.
- [25] C. Szegedy, V. Vanhoucke, S. Ioffe, J. Shlens, Z. Wojna, Rethinking the inception architecture for computer vision, in: *The IEEE Conference on Computer Vision and Pattern Recognition (CVPR)*, 2016.

- [26] B. Zoph, V. Vasudevan, J. Shlens, Q. V. Le, Learning transferable architectures for scalable image recognition, in: Proceedings of the IEEE conference on computer vision and pattern recognition, 2018, pp. 8697–8710.
- [27] A. G. Howard, M. Zhu, B. Chen, D. Kalenichenko, W. Wang, T. Weyand, M. Andreetto, H. Adam, Mobilenets: Efficient convolutional neural networks for mobile vision applications, cite arxiv:1704.04861 (2017).
URL <http://arxiv.org/abs/1704.04861>

Appendixes

Table 6: Problems, class names, and term IDs from the data set used.

	normal	blur	polyp	cancer	ulcer	blood	inflammation	Crohn	diverticulum	varicose
10-CLASS	b02, h	q02, q05, q07, q09	c22, g14, g31, g45	c05, g11, g26, g39	c26, c27, c32, g18, g05, g19, g50, g51, g52	b01, c02, c05, g18, g08, g19, g39, g51	c03, c25, c34, g18, g20, g22, g54, g56, g59, g67	c16, c32, g03, g09, g23, g33, g35, g44, g70	c17, c31, g09, g24, g29, g40, g41	g36, g53
5-CLASS	normal	polyp	cancer	ulcer	blood					
	b02, h	c22, g14, g31, g45	c05, g11, g26, g39	c26, c27, c32, g18, g05, g19, g50, g51, g52	b01, c02, c05, g18, g08, g19, g39, g51					
2-CLASS BLUR	normal	disease								
	b02, h	b01, c, g								
	blur	sharp								
	q02, q05, q07, q09	b, c, g, q01								

Table 7: Number of used images (patients in parentheses) for each problem and variant.

10-CLASS	normal	blur	polyp	cancer	ulcer	blood	inflammation	Crohn	diverticulum	varicose
Precise	1022 (69)	589 (75)	1192 (339)	688 (151)	567 (197)	769 (194)	805 (267)	84 (27)	135 (50)	252 (85)
Imprecise	17888 (113)	28145 (190)	6648 (339)	19569 (152)	3324 (197)	19717 (195)	13768 (268)	372 (27)	626 (50)	1111 (85)
5-CLASS	normal	polyp	cancer	ulcer	blood					
Precise	1022 (69)	1192 (339)	688 (151)	567 (197)	769 (194)					
Imprecise	17888 (113)	6648 (339)	19569 (152)	3324 (197)	19717 (195)					
2-CLASS	normal	disease								
Precise	1022 (69)	3980 (1070)								
Imprecise	17888 (113)	46156 (1071)								
BLUR	blur	sharp								
Precise	589 (75)	4866 (1091)								
Imprecise	28145 (190)	63869 (1102)								

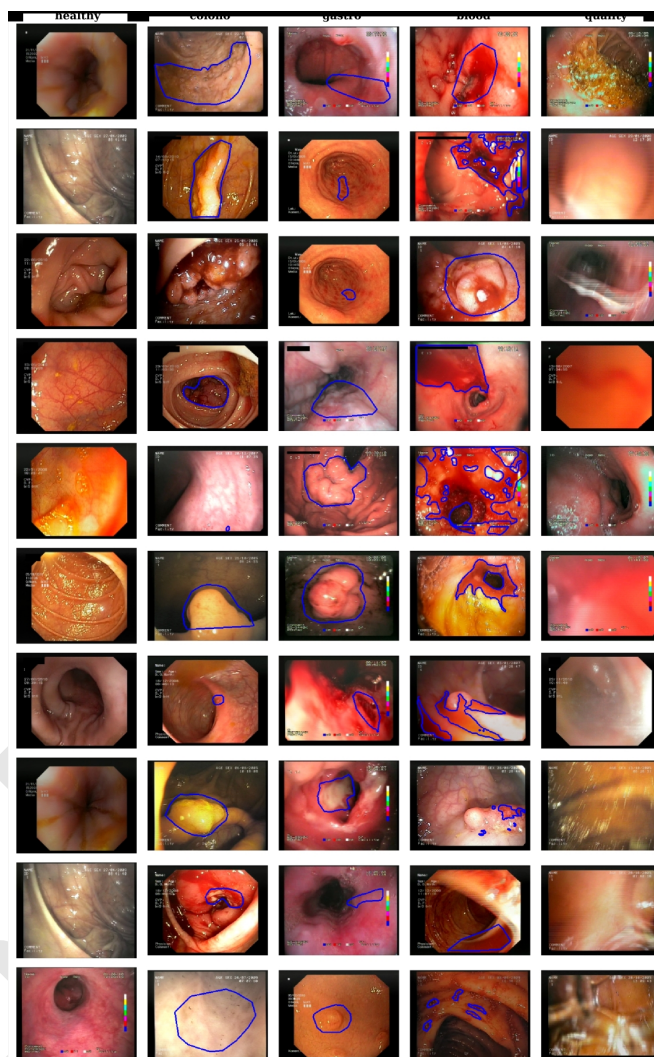


Figure 6: Examples of images (and annotation masks – as blue contours) in the data set